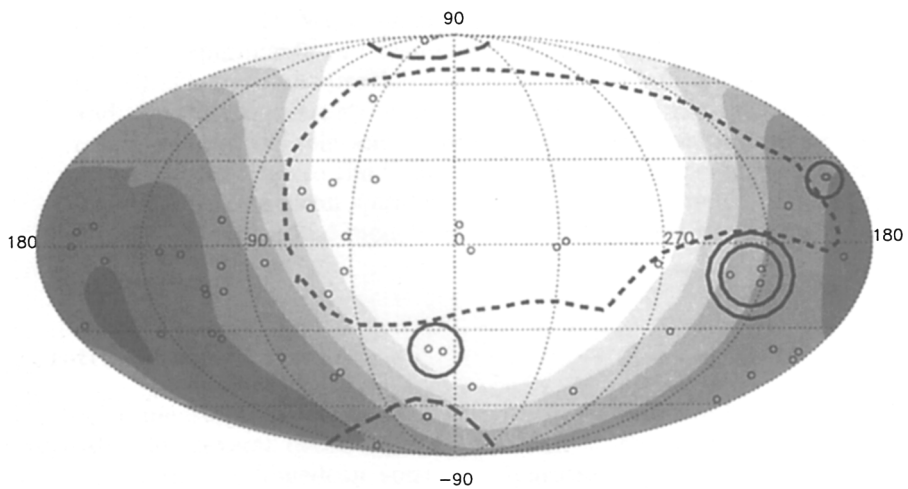


# Session VII

## Energetic Particles and the Local Interstellar Medium



Projection of the LIC model on the sky in Galactic coordinates. The shadings indicate the values of  $N_{\text{HI}}$  in units of  $10^{18} \text{ cm}^{-2}$  from the Sun to the edge of the LIC. From darkest to lightest, the shadings designate  $> 2.0$ ,  $1.0\text{--}2.0$ ,  $0.5\text{--}1.0$ ,  $0.25\text{--}0.5$ ,  $0.10\text{--}0.25$ ,  $0.05\text{--}0.10$ , and  $< 0.05$  in these units. The large dashed contour indicates the location of the G cloud, and the smaller dashed contours indicate the locations of the North Galactic Pole and South Galactic Pole clouds. Solid lines indicate the contours of four other clouds (adapted from Linsky, p. 595).

## Heliospheric Magnetic Field Configuration and its Coronal Sources

T. H. Zurbuchen

*University of Michigan, Department of Atmospheric, Oceanic and Space Sciences, 2455 Hayward Street, Ann Arbor, MI 48109-2143, USA*

**Abstract.** The heliospheric magnetic field configuration is largely determined in the solar atmosphere. The interplanetary magnetic field is therefore intimately linked with the coronal structure and evolution during the solar cycle. We summarize recent experimental results from active satellite experiments on Ulysses and the Advanced Composition Explorer (ACE). These results provide constraints on the sources of the solar wind and also the magnetic structure of the heliosphere and the corona. These results suggest the relevance of reconnection processes and differential rotation effects close to the Sun. This leads to large perturbations from a standard Archimedean spiral configuration which cannot be successfully modeled using coronal models which assume a potential magnetic field.

### 1. Introduction

The three-dimensional magnetic structure of the heliosphere has been actively investigated for several decades. This research started with Parker's (1958) prediction of the Archimedean spiral configuration. Parker argued that the magnetic field configuration would be affected by two basic properties. First, the solar rotation winds the magnetic field, and, at the same time, the solar wind carries it radially outwards. These considerations lead to the well-known Parker magnetic field configuration:

$$\begin{aligned} B_r &= B_0(r_0/r)^2, \\ B_\theta &= 0, \\ B_\phi &= -\frac{B_0 r_0^2}{V r} \Omega \sin \theta. \end{aligned} \tag{1}$$

Here,  $B_0$  indicates the magnetic field strength at  $r_0$  close to the Sun,  $r$  stands for the heliocentric distance,  $\Omega$  and  $V$  for solar rotation and solar wind speed. The solar wind velocity is assumed to be radial for this calculation. Two aspects of Equation 1 should be pointed out. First, due to  $B_\theta = 0$ , all field lines will be confined to cones of constant latitude. Second, for most parts of the heliosphere  $B_\phi \gg B_r$ . In the ecliptic, the radial component is dominant only for  $r < 1$  AU of the Sun. Transverse components of the coronal magnetic field are therefore important to determine the large-scale magnetic structure of the heliosphere. Figure 1 summarizes a number of effects which are neglected in Equation 1. The effects close to the Sun ( $r \leq 5 R_s$ ) lead to large-scale motions of magnetic field

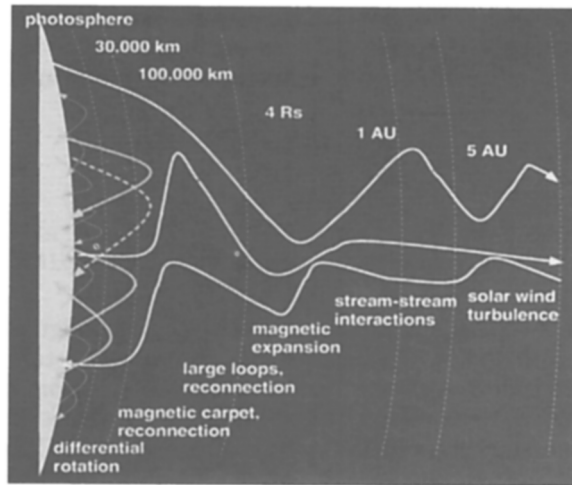


Figure 1. Schematic representation of a number of solar and heliospheric effects which can change the magnetic structure of the heliosphere.

footpoints. These motions are mapped out in the heliosphere and cause large-scale deviations from an average spiral structure. The other effects work directly on the flow, where the magnetic field is frozen in, and change the magnetic field through changes of the flow field. The processing of the solar wind from the surface to heliospheric distances of  $\sim 1$  AU or more is often the least understood link in the chain of events determining the structure and interaction of the solar wind with the Earth. This is perhaps the main reason for the increased interest in compositional data discussed in this paper. Compositional patterns reflect the solar source and are not affected by plasma interactions at  $r$  larger than a few  $R_s$ .

This paper concentrates on the processes at  $r \leq 5 R_s$ . Large-scale stream-stream interaction processes have been discussed elsewhere (Burlaga 1996). We refer to Bougeret's paper (these proceedings) for a discussion of Coronal Mass Ejections (CMEs). The limited scope of this paper prohibits the discussion of a larger number of new results. Instead, we refer the reader to three collections of recent papers on this topic (Mewaldt et al. 2000; Marsden et al. 2001; Zurbuchen et al. 2001, and references therein).

The experimental constraints on the large-scale structure of the heliosphere are fundamentally related to the following three questions:

1) *What is the source of the solar wind in the corona?* If all solar wind is associated with coronal holes (see, e.g. Bravo et al. 1997), then the solar wind properties only reflect the properties of these regions. Different sources will lead to the interesting question of how these relate to each other. Potential interaction processes will directly affect the heliospheric magnetic field.

2) *What is the underlying magnetic field configuration?* This question relates to in situ magnetic field measurements. We will argue that such measurements cannot be used in general to distinguish large-scale deviations from local turbulence. Low-energy particles in the heliosphere propagate along magnetic

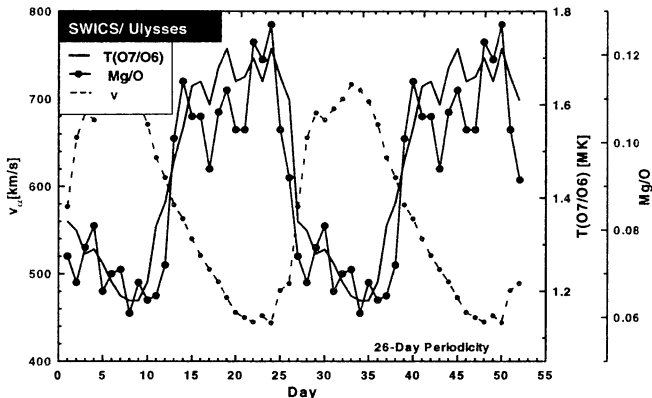


Figure 2. Superposed epoch analysis of Ulysses-SWICS speed and composition data. Coronal-hole-associated solar wind is very different from slow solar wind in all parameters. Figure after Geiss et al. (1995).

field lines. These therefore often provide better measures for the large-scale structure of the magnetic field.

3) *How do these observations relate to the remote observations of the solar corona?* Due to the lack of three-dimensional magnetic field observations in the corona, this is a non-trivial question. We will use compositional tracers to relate solar wind plasma to its coronal sources.

We will deal with the first question in section 2. Section 3 will discuss observational constraints relating to question 2. Section 4 will then put these heliospheric data into the context of coronal observations, responding to question 3. We will discuss these results and their interpretation in Section 5.

## 2. Sources of the Solar Wind

This topic has been the focus of a large number of heliospheric investigations during the past decades (see, Schwenn 1990, and references therein). However, it has been impossible to conclusively answer the questions about the coronal sources of the slow solar wind. Recent instrumentation, such as the Solar Wind Ion and Composition Spectrometer (SWICS) on Ulysses, have added crucial constraints to solar wind theories. One key result from that data is presented in Figure 2 which shows a superposed epoch analysis of solar wind speed (from  $\text{He}^{2+}$ ), O freeze-in temperature, and the elemental abundance ratio Mg/O. The O freeze-in temperature is determined from  $n_{\text{O}^{+7}}/n_{\text{O}^{+6}}$  under local thermal equilibrium assumptions (for details, see Geiss et al. 1995).

It is obvious from Figure 2 that there are two fundamentally different types of steady solar wind flows (Schwenn 1990). Fast solar wind is associated with relatively cool regions on the Sun, coronal holes, and therefore has low freeze-in temperatures, as expected. Slow solar wind is fundamentally different in character as seen in a change of freeze-in temperature and elemental composition. A detailed investigation reveals that slow solar wind shows an enhancement of

all elements with a low ( $< 10$  eV) First Ionization Potential (FIP) (von Steiger et al. 1997).

It is obvious from Figure 2 that there are differences in the transition time scales of the leading and trailing edge of the fast solar wind stream. Posner et al. (2001) have recently shown that this is caused by the heliospheric stream-stream interactions which tend to steepen the transition at the leading edge, and flatten it at the trailing edge. When mapped back to the Sun both transitions occur within  $\sim 1^\circ$ - $2^\circ$ . This finite width is well explained by field-aligned mixing at the interface of the two solar wind regimes. This suggests the importance of magnetic connections between the two solar wind regimes. For a detailed discussion refer to Zurbuchen et al., 1999.

The low-latitude, predominantly slow solar wind has been studied for over two solar cycles. Many relevant results concerning its magnetic field and plasma properties can be found in other reviews and are not discussed in detail here. Generally, slow solar wind associated with streamers is more variable than coronal hole solar wind (Gosling 1996). This variability has often been attributed to interaction processes in the heliosphere. A recent study of compositional data from ACE-SWICS with time resolutions of 12 min has shown that this variability is intrinsically solar in nature. The freeze-in ratio  $n_{O+7}/n_{O+6}$  is observed to vary quite substantially, with sharp transitions about every 10 hrs. Such transitions occur even though the magnetic polarity does not switch. The slow solar wind appears to be quite variable, derived from several sources. Similar variations are also observed in the elemental composition.

The data discussed so far have been gathered close to activity minimum. Figure 3 shows a time period of solar wind in March 1999, combining solar observations from SOHO-EIT, approximate coronal hole locations based on He10830 A from March 11, and ACE observations in March 1999. We show solar wind speed,  $n_{O+7}/n_{O+6}$ , the average Fe charge state, and the magnetic winding angle ( $\phi$ ) as a measure for the magnetic field polarity. The solar wind speed fluctuates between 300 and 600 km/s. It is difficult to identify coronal-hole-associated solar wind based on the speed signatures. The magnetic polarity changes from positive to negative and back to positive after approximately 10 days. The coronal hole association is most easily tested using  $n_{O+7}/n_{O+6}$ . Around day 71 (March 12) the  $n_{O+7}/n_{O+6}$  drops below 0.1, and recovers around day 78 (March 19). This therefore identifies solar wind from a coronal hole with positive magnetic polarity. Another coronal-hole-associated wind with negative polarity is observed around day 62.

The low  $n_{O+7}/n_{O+6}$  signature can be successfully applied to the identification of coronal-hole-associated plasma. Periods of low  $n_{O+7}/n_{O+6}$  can be directly linked to coronal-hole-associated wind until solar maximum (Zurbuchen et al. 2000b). The ratio  $n_{O+7}/n_{O+6}$  is much lower within polar coronal holes than in equatorial holes. However, the elemental signatures remain the same. Also, slow solar wind is more fractionated than fast solar wind, as shown in Figure 2. For a more detailed discussion refer to Zurbuchen et al. (2000b).

We therefore conclude that there are two types of solar wind during the entire solar cycle. Even though solar wind streams from coronal holes exhibit large variations in speed, density, and temperature, their compositional signatures are nonetheless unambiguous. There is also solar wind originating from

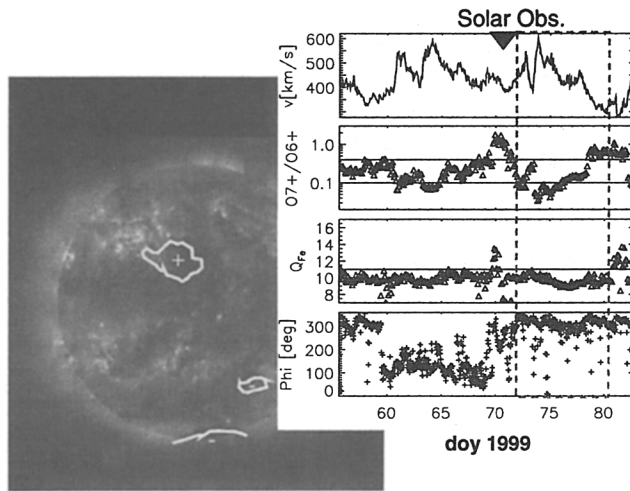


Figure 3. The identification of solar wind from low-latitude coronal holes. An EIT image of March 11, 1999 is shown, superposed are the coronal hole boundaries from He 10830. This coronal hole gives rise to the moderately fast stream with a clear depletion of  $n_{O^{+7}}/n_{O^{+6}} < 0.1$  and the expected polarity. For details refer to text.

other than coronal holes. This wind is identified based on its large variability and particularly by its enhanced FIP-fractionation.

### 3. Magnetic Field Structure

Equation 1 has been successfully tested in many experimental studies from 0.3 AU to 70 AU (see, e.g., Mariani & Neubauer, 1990). It tends to be a good approximation for long-term averages of the magnetic field measurements. However, the deviations from that average are substantial. It is difficult to determine locally whether these deviations are due to turbulence or if are caused by random or systematic motions close to the Sun. This is demonstrated in Figure 4. Two clearly different heliospheric field configurations are shown on the left-hand side (Parker 1958; Fisk 1996 using the approximation from Zurbuchen et al. 1997). Fisk's field configuration includes the footpoint motions caused by differential rotation and magnetic expansion typical for the declining phase of the solar activity cycle. Spacecraft measurements are simulated at latitudes from  $65^\circ$  to  $85^\circ$ , similar to the Ulysses high-latitude pass in 1993-1994. For these simulations, we assumed a turbulence level similar to the one observed by Balogh et al. (1995) using Ulysses data at high latitudes. Figure 4 demonstrates how difficult it is to extract the large-scale magnetic field configuration from a one-point measurement in the heliosphere. Even though the two field configurations are very different, no significant deviations are seen in a local measurement. Particularly, a histogram, such as shown in Figure 4 will tend to average out important phase differences in the two field configurations. The identification of such effects is much easier in a more symmetric and steady configuration such as during the second high-latitude pass of Ulysses in 1995-1996. During this time period the



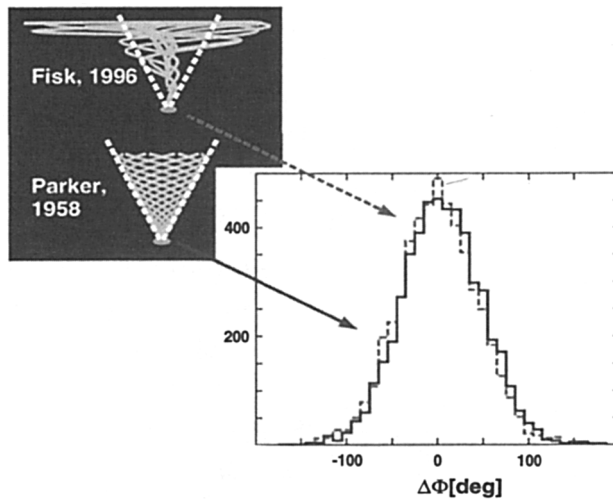


Figure 4. In situ tests of two different heliospheric field configurations. The left-hand side shows two configurations proposed by Fisk (1996) and Parker (1958). The right-hand side shows simulated in situ measurements for these two simulations.  $\Delta\Phi$  is the local deviation from the Parker angle.

average magnetic field direction is clearly observed to be underwound during most parts of the high-latitude corona. The amount of underwinding agrees with the differential rotation of the high-latitude corona (Banaszkiewicz et al. 1998). This is significant signature for the importance of differential rotation effects in the outer corona. Other secondary indications have been discussed by Forsyth et al. (1995) and Zurbuchen et al. (1997). The reconnection processes associated with the emergence and merging of small flux elements (“magnetic carpet”), described by Schrijver et al. [1997], are not big enough to eliminate the systematic motion of the differential rotation (Fisk et al. 2001).

One of the most unexpected discoveries of the Ulysses mission is the observation of recurrent events of low-rigidity particles observed up to very high latitudes (Roelof et al. 1997; Simnett et al. 1995). These particles are accelerated at low latitude Co-Rotating Interaction Regions (CIRs) and propagate along heliospheric magnetic field lines. These particles were observed up to the highest Ulysses latitudes with the same typical clock-angle dependence of CIRs. The particles in these recurrent events were observed to stream towards the Sun, suggesting direct magnetic connection to low latitudes. Such systematic motions are inconsistent with Parker’s configuration given in Equation 1 because they involve substantial  $B_\theta$ -components. It has also been pointed out by Simnett et al. (1995) that the observed profiles of the particle recurrences exclude an explanation based solely on random motions of the magnetic field due to turbulence in the heliosphere or close to the Sun. The  $B_\theta$ -components have to be systematic and substantial in size. This has been explained using a field configuration shown in the upper right corner of Figure 4. For a detailed discussion of this configuration refer to Fisk et al. (1996).

Energetic particles are also a very good tool to explore the large-scale magnetic structure of the low-latitude solar wind. The propagation of energetic particles from localized events close to the Sun reflects the detailed structure of the interplanetary medium (Mazur et al. 2000). Impulsive particle events from one single solar source often have short time scale (3-hr) variations in their intensity that occur simultaneously across all energies. These features are most likely caused by the convection of magnetic flux tubes past the observer that are alternately filled and empty of flare ions even though they have a common flare source at the Sun. This reflects a very granular distribution of magnetic flux tubes. These tubes disintegrate with increasing distance from the Sun due to turbulence effects in the heliosphere (Goldstein et al. 1995).

We therefore conclude that there have been observations of significant deviations from an average Parker model. These deviations are systematic in nature and can be traced to differential rotation effects close to the Sun. Such systematic variations are only easily observed in situ if the heliosphere has a lot of symmetry. However, they may be present all the time. The low-latitude solar wind has a structure which is very granular, made up of “bottles” or flux tubes which are identified best through observations of low-energy particles.

#### 4. Connection to Coronal Structure

These observations are now put in context of the magnetic field structure in the corona. There are solar motions and processes that are not captured by Equation 1. Using a result by Hollweg & Lee (1989), Equation 1 can be generalized to include any perpendicular motions of the magnetic field footpoints  $\mathbf{u}_\perp$ . Such footpoint motions result in magnetic field perturbations in the solar wind according to Equation 2.

$$\mathbf{B}_\perp = -\mathbf{u}_\perp(r/r_s)B_r/V. \quad (2)$$

Here,  $r_s$  denotes the heliocentric distance where  $\mathbf{u}$  is measured. Obviously, if  $\mathbf{u}_\perp = \Omega \sin \theta \mathbf{e}_\phi$ , Equation 2 reduces to Parker’s field configuration. Motions associated with solar processes, such as reconnection or differential rotation will result in non-zero  $\mathbf{u}_\perp$  which will map into the heliosphere. Such changes will affect the large-scale structure and can have a large impact on energetic particle transport in the heliosphere. Our discussion in this section will therefore concentrate on the nature of such motions in the solar wind regimes discussed above. For a detailed discussion of the theoretical arguments leading to these motions, refer to Fisk (2001).

##### 4.1. Fast Solar Wind

We have already mentioned that there is little argument that this wind is originating exclusively from coronal holes. Recently, Woo, & Habbal (1999) have advocated that the solar wind could also originate from different regions. However, we believe that such an assumption can be safely excluded based on the composition of this plasma. Magnetic field lines in the fast solar wind (or, “not-so-fast” coronal-hole-associated solar wind during activity maximum) are directly attached to the photospheric magnetic elements within coronal holes.



Most of these elements are associated with closed magnetic field short loops which never make it out of the solar atmosphere into the heliosphere. The footpoints of the open field lines certainly interact with these magnetic flux elements, which results in random footpoint motions (Jokipii & Parker 1969). However, these random effects are not as fast as the differential rotation effects which systematically transport these field lines around (Fisk 2001).

During times in the solar cycle with large polar coronal holes, these differential rotation effects are very important in shaping the large-scale heliospheric field. Due to the magnetic expansion of these field lines, these effects produce systematic motions in the latitude, which result in  $B_\theta$  components (Fisk 1996; Zurbuchen et al. 1997). The resulting field configuration is shown in the top-panel of the left-hand side of Figure 4.

#### 4.2. Slow, Fractionated Solar Wind

Many sources with different compositional characteristics contribute to the highly variable flow of slow, fractionated solar wind. A very interesting observation relative to the origin of the slow solar wind recently came from the comparison of the elemental abundance of slow solar wind and remote solar observations. Feldman & Widing (1999) have reported on remote observations of elemental fractionation in closed magnetic structures: When loops emerge from the photosphere, they have a composition which is very similar to the average photosphere. In relatively large loops ( $> 10^5$  km) elemental fractionation is then observed to happen on a time scale of  $10^5 - 10^6$  s, biasing towards elements with low ( $< 10$  eV) first ionization potential. This naturally suggests a direct relationship between coronal loops and the slow solar wind. Somehow, the fractionated loop material is released into the heliosphere, presumably through reconnection. A possible process responsible for the elemental abundance enhancements must depend on the physics of these large loops. Such a process was predicted by Zurbuchen et al. (1998) and by Schwadron et al. (1999).

Such a concept is also consistent with observations from energetic particles, as discussed above. The reconnection processes responsible for releasing the plasma into the heliosphere will produce relatively random magnetic field linkages over large distances in the solar corona. This will lead to substantial diffusion perpendicular to the magnetic field (Giacalone et al. 2000).

The footpoint motion also crosses from fast to slow solar wind, as suggested by the finite width of the compositional transition. This naturally couples the two regimes (Fisk et al. 1999). Close to activity minimum, for example, the reconnection processes at low latitudes must, on the average, respond to the effects of the differential rotation at high latitudes. Close to activity maximum, the large-scale polarity shift of the underlying photosphere will tend to favor certain reconnection geometries over others. For a detailed discussion of the solar wind structure refer to Zurbuchen et al. (2000a). For a discussion of the reconnection processes at low latitudes and their relation to the high-latitude corona, refer to Fisk et al. (1999).

## 5. Discussion

The importance of footpoint motions for the determination of the heliospheric magnetic field has become evident in recent observations. Such motions can not be captured in simulations which assume a potential field configuration in the corona (Schulz, 2001; Wang & Sheeley, 1992). Such simulations typically assume a radial magnetic field on a surface at  $\sim 2 R_s$ . Any systematic or random motions resulting in magnetic field perturbations are therefore suppressed by such calculations. The future of research in this field will likely involve realistic time-dependent MHD calculations of the coronal structure.

The new instrumentation on recent spacecraft have answered some very old questions. These results connect areas which did not seem to have anything to do with each other. We will only be able to prove the validity of some of these connections based on results from a new generation of remote and in situ experiments.

**Acknowledgments.** We thank L. A. Fisk and N. A. Schwadron for many useful discussions. We acknowledge the use of ACE-SWICS, ACE-MAG, SOHO-EIT and Kitt Peak Coronal Hole data. This work was supported, in part, by NASA contracts NAG5-2810 and NAG5-7111.

## References

- Balogh, A., et al. 1995, *Sci*, 268, 1007  
Banaszkiewicz, M., Axford, W. I., & McKenzie, J. F. 1998, *A & A*, 337, 940  
Bravo, S., & Stewart, G. A. 1997, *ApJ*, 489, 992  
Burlaga, L. F., Ness, N. F., Belcher, J. W., Lazarus, A. J., & Richardson, J. D. 1996, *Space Sci. Rev.*, 78, 33  
Feldman, U., Widing, K. G., & Warren, H. P. 1999, *ApJ*, 522, 1133  
Fisk, L. A., 1996, *JGR*, 101, 15,547  
Fisk, L. A., Zurbuchen, T. H. & Schwadron, N. A. 1999, *JGR*, 521, 868  
Fisk, L.A. 2001, *JGR*, in press  
Forsyth, R. J., et al. 1995, *GRL*, 22, 3321  
Geiss, J., Gloeckler, G., & von Steiger, R. 1995, *Space Sci. Rev.*, 72, 49  
Giacalone, J., Jokipii, J. R., & Mazur, J. E. 2000, *ApJ*, 532L, 75  
Gloeckler, G., et al. 1998, *Sp. Sci. Rev.* 86, 495  
Goldstein, M. L., Roberts, D. A., & Matthaeus, W. H. 1995, *ARA&A*, 33, 283  
Gosling, J. T. 1996, in *AIP Conf. Proc.*, 385, *Robotic Exploration close to the Sun: Scientific Basis*, ed S. R. Habbal  
Hollweg, J. V., & Lee, M. A. 1989, *GRL*, 16, 919  
Jokipii, J. R., & Parker, E. N. 1969, *ApJ*, 155, 777  
Linker, J. A., et al. 1999, *JGR*, 404, 9808L  
Mariani, F., & Neubauer, F.M. 1990, in *Physics of the inner Heliosphere I*, eds. R. Schwenn and E. Marsch (Springer Verlag) 183

- Marsden R. (ed) 2001, *ESLAB Symp. Proc.* 34, The 3-D heliosphere at solar maximum
- Mazur, J. E., et al. 2000, *ApJ*, 532L, 79
- Mewaldt, R. A. et al. (eds) 2000, *AIP Conf Proc.* 528, Acceleration and transport of energetic particles in the heliosphere
- Parker, E. N. 1958, *ApJ*, 128, 664
- Posner, A., et al. 2001, *JGR*, in press
- Roelof, E. C., et al. 1997, *JGR*, 102, 251
- Schrijver, C. J. et al. 1997, *ApJ*, 487, 424
- Schulz, M. 2001, *JGR*, in press
- Schwadron, N. A., Fisk, L.A., & Zurbuchen, T. H. 1999, *ApJ*, 521, 859
- Schwenn, R 1990, in *Physics of the inner Heliosphere I*, eds. R. Schwenn & E. Marsch (Springer Verlag) 99
- Simnett, G. M., Sayle, K. A., Tappin, S. J., & Roelof, E. C. 1995, *Space Sci. Rev.*, 72, 327
- von Steiger, R., Geiss, J., & Gloeckler, G. 1997 in *Cosmic winds and the heliosphere* (Arizona Press) 581
- Wang, Y.-M., & Sheeley, N. R., Jr. 1992, *ApJ*, 401, 378
- Woo, R., & Habbal, S. R. 1999, *GRL*, 26, 1793.
- Zurbuchen, T. H., Schwadron, N. A., and Fisk, L. A. 1997, *JGR*, 102, 24,175
- Zurbuchen, T. H., Fisk, L. A., Gloeckler, G., & Schwadron, N. A. 1998, *Space Sci. Rev.*, 85, 397
- Zurbuchen, T. H., Hefti, S., Fisk, L. A., Gloeckler, G., & von Steiger, R. 1999, *Space Sci. Rev.*, 87, 353
- Zurbuchen, T. H., Hefti, S., Fisk, L. A., Gloeckler, G. & Schwadron, N. A. 2000a, *JGR*, 105, 18,327
- Zurbuchen, T. H., et al. 2000b, *JGR*, in press
- Zurbuchen, T. H., Jokipii, J. R., & Belcher J. W. 2001, *JGR*, in press